Immunity
Article

T Lymphocytes Negatively Regulate Lymph Node Lymphatic Vessel Formation

Raghu P. Kataru,[1,2,6] Honsoul Kim,[1,2,6] Cholsoon Jang,[1,3] Dong Kyu Choi,[1,3] Bong Ihn Koh,[1,2] Minah Kim,[1,3] Sudheer Gollamudi,[1,3] Yun-Keun Kim,[5] Seung-Hyo Lee,[2,*] and Gou Young Koh[1,2,3,4,*]
[1]National Research Laboratory of Vascular Biology
[2]Graduate School of Medical Science and Engineering
[3]Department of Biological Sciences
[4]Graduate School of Nanoscience & Technology (WCU)
Korea Advanced Institute of Science and Technology (KAIST), Daejeon, 305-701, Korea
[5]Department of Life Science and Division of Molecular and Life Sciences, Pohang University of Science and Technology, Pohang, 790-784, Korea
[6]These authors contributed equally to this work
*Correspondence: seung-hyo.lee@kaist.ac.kr (S.-H.L.), gykoh@kaist.ac.kr (G.Y.K.)
DOI 10.1016/j.immuni.2010.12.016

SUMMARY

Lymph node lymphatic vessels (LNLVs) serve as a conduit to drain antigens from peripheral tissues to within the lymph nodes. LNLV density is known to be positively regulated by vascular endothelial growth factors secreted by B cells, macrophages, and dendritic cells (DCs). Here, we show that LNLV formation was negatively regulated by T cells. In both steady and inflammatory states, the density of LNLVs was increased in the absence of T cells but decreased when T cells were restored. Interferon-γ secretion by T cells suppressed lymphatic-specific genes in lymphatic endothelial cells and consequently caused marked reduction in LNLV formation. When T cells were depleted, recruitment of antigen-carrying DCs to LNs was augmented, reflecting a compensatory mechanism for antigen presentation to T cells through increased LNLVs. Thus, T cells maintain the homeostatic balance of LNLV density through a negative paracrine action of interferon-γ.

INTRODUCTION

Lymph nodes (LNs) are immunological junctions strategically situated throughout the mammalian body at sites where soluble and cell-mediated antigens drain from peripheral tissues. At these specific locations, the antigens are exposed to specific lymphocytes, enabling the latter to generate adaptive immune responses (Drayton et al., 2006; Gretz et al., 1997; Randolph et al., 2005). LNs contain a network of lymphatic vessels (LVs) that are used as a route for antigen delivery. The microstructure of LNLVs consists of sinusoidal extensions that begin at the peripheral afferent LVs, are further distributed just below the capsule and surrounding B cell follicles, and stretch toward the medullar region of LNs (Drayton et al., 2006; Mueller and Germain, 2009). LNLVs function as specialized conduits for carrying peripheral tissue-borne and cell-mediated antigen into physical proximity of the T cell zone. Thus, rapidly moving T cells can encounter their specific antigen to initiate adaptive immune responses (Alvarez et al., 2008; Catron et al., 2004; Itano and Jenkins, 2003; Junt et al., 2008; von Andrian and Mempel, 2003). From this point of view, LNLVs are critical in providing an interface between antigen-presenting cells (APCs) and T cells. Therefore, it can be deduced that the density of LNLVs, the number of T cells, or both might act as rate-limiting determinants of antigen presentation and immune reaction initiation. However, little is known about the relationship between LNLVs and T cells in the complex micro-architecture of LNs.

We, along with several groups, have reported that peripheral inflammation transiently induces robust lymphangiogenesis in draining LNs (Halin et al., 2007; Kataru et al., 2009; Liao and Ruddle, 2006). In the process of LN lymphangiogenesis, LNLVs below the capsule proliferate, grow, and penetrate deep into the cortex. This LN lymphangiogenesis is thought to be mediated mostly by vascular endothelial growth factors (VEGFs), including VEGF-A, -C, and -D secreted at the site of inflammation (Halin et al., 2007; Kataru et al., 2009). Various intranodal cellular components are deeply involved in the process of inflammatory LN lymphangiogenesis by secreting VEGFs. For instance, during the process of inflammation, intranodal B cells secrete VEGF-A (Angeli et al., 2006) and $CD11b^+$ macrophages migrated from peripheral tissues secrete VEGFs, which promote intranodal lymphangiogenesis (Kataru et al., 2009; Kim et al., 2009). Furthermore, stromal fibroblastic reticular cells (FRCs) in LNs are known to influence the LN vasculature by secreting VEGFs in both homeostatic and inflammatory conditions (Chyou et al., 2008). However, the role of T cells in regulating LNLVs has not been clarified. Considering that T cells constitute more than half of the total LN cellularity and are the major effector cells that interact with DCs migrating through LVs, it is intriguing whether they have any effect on LNLVs.

During acute inflammation, LN remodeling is characterized by a transient increase in size, cellularity, lymph and blood flow, blood vessel, and high endothelial venule density (Drayton et al., 2006). LNLVs also expand transiently and regress back to normal as inflammation resolves (Kataru et al., 2009). However, there is little data regarding how the LNLVs expand and retreat as inflammation evolves. We thought it would be

particularly interesting to see whether there is a correlation between the regression of LNLVs and alterations of the profile of lymphocyte populations during the resolving stage of inflammation. In our study, we observed that as inflammation progress, dynamic remodeling of LN microarchitecture takes place. At the peak of inflammation, LNLVs were found to penetrate deep into the T cell zone (paracortex and cortex), but once the inflammation had resolved, their regression was observed. Consequently, LNLVs would have had to trespass the T cell zone during the peak of inflammation, theoretically suggesting a possibility of a yet unknown reciprocal influence that might define an intimate relationship between LNLVs and the T cell population.

Interferon-γ (IFN-γ) is a pleiotropic cytokine secreted from type 1 helper T (Th1) cells and plays a major role in initiating cell-mediated adaptive immune responses as well as in modulating cell growth and differentiation (Dalton et al., 1993). IFN-γ plays a vital role during viral infection in regulating the number of T cells, particularly $CD8^+$ T cells (Tewari et al., 2007; Whitmire et al., 2005). Several reports indicate that IFN-γ has a strong antiangiogenic effect causing tumor blood vessel regression (Fathallah-Shaykh et al., 2000; Gately et al., 1994; Ruegg et al., 1998). Furthermore, the blood vessel regression observed during tumor immunotherapy is mainly attributed to IFN-γ secreted by T cells located in and around the tumor microenvironment (Ibe et al., 2001). However, the effect of IFN-γ on LVs is poorly understood with only limited in vitro data indicating that IFN-γ may have an antilymphangiogenic role (Shao and Liu, 2006). Considering the strong antiangiogenic property of IFN-γ and the intersecting pathways of blood and lymphatic vessels, we hypothesized that IFN-γ could have an antilymphatic effect. To test this hypothesis, we have analyzed LNLVs under several T cell-deficient conditions. Our findings revealed that T cells negatively regulate LNLVs, and IFN-γ was deeply involved in the process by acting as a strong antilymphatic component of the LN microenvironment. Thus, in combination with the already known prolymphatic effect of B cells, the antilymphatic role of T cells that we describe here accounts for a balanced intranodal regulatory mechanism that provides us with an insight on how LNLV formation is controlled.

RESULTS

T Cell-Deficient Athymic Mice Have Abundant LNLVs

Normal mice cervical LN sections (Figure S1A available online) were immunostained for CD3ε (Pan T cell marker), B220 (B cell marker), and LYVE-1 (lymphatic vessel marker) to delineate the T cell zone, B cell zone, and LVs, respectively (Figure 1A; Figure S1B). $LYVE\text{-}1^+$ LVs were observed mainly in the subcapsular regions and extended to the medullary regions. In contrast, LVs were very scarce or absent in the T cell-rich paracortex, which occupied a considerable portion of the LNs (Figure S1B). Higher-magnification images revealed that LVs were closely associated to regions populated with B cells but not with T cells (Figure S1C). This observation led us to question why T cell-rich areas do not accommodate LVs.

To address the question, we explored the distribution profile of LVs in T cell-deficient LNs retrieved from athymic mice. LNs from four representative areas, namely cervical (cLN), inguinal (iLN), mesenteric (mLN), and axillary (aLN) regions, were obtained. The LNs of athymic mice displayed a higher density of $LYVE\text{-}1^+$ LVs (~2.4- to 3.9-fold higher) (Figures 1A and 1B), larger size (Figure 1C), and the absence of T cells (Figure 1D) compared to those of normal mice. To obtain quantitative measurements of lymphatic endothelial cell (LEC) count in LNs, flow cytometry analysis of dissociated LNs was performed (Figures 1E and 1F). The results of flow cytometry were reproducible in a profile that positively correlated with our LNLV density measurements, verifying the reliability of our immunohistochemical data. The LNLVs of athymic mice densely covered the entire T cell-absent LN paracortex, a corresponding region where LNLVs were scarcely populated in normal mice (Figure 1A). Coimmunostaining for Prox-1 (a master transcriptional factor of lymphatic differentiation) and LYVE-1 revealed that the examined $LYVE\text{-}1^+$ vessel-like structures were also $Prox\text{-}1^+$, confirming their identity as LVs (Figure 1G). These results suggest that the distribution of LNLVs is inversely correlated with that of T cells.

$CD4^+$ and $CD8^+$ T Cells but Not $B220^+$ B Cells Suppress LNLVs

We wondered whether the LNLVs of athymic mice would resemble those of normal mice if they were provided with T cells. $CD4^+$ and $CD8^+$ T cells were obtained from ds-Red (variant of red fluorescent protein) mice and each type of T cell was independently transferred into athymic mice. For comparison, equal numbers of $B220^+$ B cells from ds-Red mice were adoptively transferred into athymic mice. Two days after transfer, red fluorescent $CD4^+$ or $CD8^+$ cells around T cell zones and $B220^+$ cells at germinal center regions were found in all major LNs, showing targeted homing of lymphocytes (Figure 2A). In this condition, LNLVs were significantly diminished in the areas occupied by either $CD4^+$ or $CD8^+$ ds-Red T cells compared with the LNs of PBS-treated mice (~20% and ~31% reduction for $CD4^+$ and $CD8^+$ T cells, respectively) (Figures 2A and 2B). However, the LV density around B cell zones was similar between control and postadoptive transfer of $B220^+$ cells (Figure 2A). Flow cytometry analysis of dissociated LNs displayed a similar profile: the LEC count was significantly decreased in mice in which either $CD4^+$ or $CD8^+$ T cells, but not $B220^+$ cells, were adoptively transferred (Figure 2C). To administer specific stimuli, we pretreated $B220^+$ B cells and both T cell subsets with PMA and ionomycin and repeated the adoptive transfer into athymic mice. Under this condition, the decrease in the LNLV density caused by the stimulated T cell subsets became more prominent (~43% and 55% reduction for $CD4^+$ and $CD8^+$ T cells, respectively). This pattern of LNLV suppression was also observed by flow cytometry analysis; LEC count decreased by adoptive transfer of either type of T cells but not by B cells (Figures 2C and 2D). These data indicate that adoptive transfer of T cells is sufficient to decrease LNLVs, supporting the hypothesis that the presence of T cells correlates with LNLV regression.

Reversible Changes of LNLVs after Depletion and Restoration of T Cells

To further specify the suppressive role of T cells in LNLVs, we induced T cell depletion (T-De) in LNs by treating the mice intravenously with anti-CD3ε (1 mg/kg/day for 5 days). This procedure successfully removed the T cells from LNs (~90%

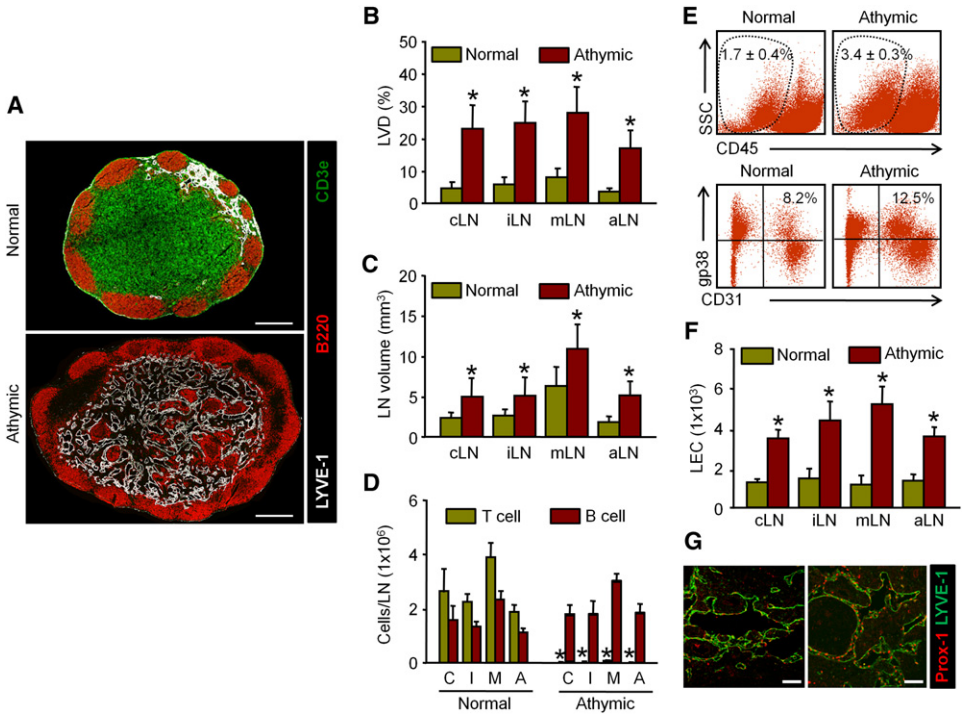

Figure 1. Athymic Nude Mice Have Abundant LNLVs

Cervical LNs (cLN, C), inguinal LNs (iLN, I), mesenteric LNs (mLN, M), and axillary LNs (aLN, A) were sampled from 8-week-old normal and athymic BALB/c mice.

(A) Representative immunohistochemistry images showing the distributions of CD3ε$^+$ T cells, B220$^+$ B cells, and LYVE-1$^+$ LVs in the midsection of cLN from n = 5 in two independent experiments. Scale bars represent 500 μm.

(B) Comparison of LV density (LVD) (n = 5 per group in two independent experiments).

(C) Comparison of LN volume (n = 5 per group in two independent experiments).

(D) Comparison of numbers of T and B cells (n = 5 per group in two independent experiments).

(E) Flow cytometry analysis of the dissociated cLN for CD45$^-$ stromal cells (top) and gp38$^+$CD31$^+$ LEC population (bottom) (n = 3 per group in two independent experiments).

(F) Comparison of LEC count per 1 × 10^6 LN cells (n = 3 per group in two independent experiments).

(G) Representative images showing LYVE-1$^+$Prox-1$^+$ LVs in the midsections of cLN from n = 3 in two independent experiments. Scale bars represent 50 μm.

The graphs show mean ± SD. *$p < 0.05$ versus normal. See also Figure S1.

depletion), whereas the LN size, density of LNLVs, and LEC percentage significantly increased (~3.7- and 3.1-fold increase of LNLV density in cLN and mLN, respectively, compared to the control group) (Figures 3A–3E) to resemble the profile of LNs from athymic mice. We then asked whether T cell restoration (T-Re) could reverse the pattern of LNLVs back to baseline. After anti-CD3e treatment, the mice were left untreated for 10 days to allow T cell recovery (~92% of control) (Figure 3B). As a result, the LNLV pattern almost returned to the baseline state (Figures 3A, 3C, and 3E), indicating that T cells have negative influence on LNLV growth.

Based on these findings, we speculated that one or more cytokines secreted by the T cells might interfere with LNLV growth. Among the cytokines secreted by T cells, IFN-γ is well known for its antiangiogenic effect (Ruegg et al., 1998). Therefore, we reasoned that the role of IFN-γ could be overlapping in function to cause an antilymphangiogenic effect and thus may be responsible for the T cell-mediated negative regulation of LNLV growth as well. To investigate this possibility, quantitative real-time PCR (qRT-PCR) of LN tissues was performed. Significant downregulation of IFN-γ mRNA in LNs of the athymic and T-De mice was observed, whereas no noticeable differences were detected between T-Re and control mice (Figure 3F), suggesting that the IFN-γ amount in LNs is mainly determined by T cells and is inversely correlated with the LNLV density. Meanwhile, the mRNA expression of VEGF-A, -C, and -D was upregulated in LNs of the athymic and T-De mice (Figure 3F) and positively correlated with the LNLV density. The amount of IFN-γ, which correlates positively to the number of T cells but negatively to the LNLV density, supports our hypothesis that T cell-secreted IFN-γ has an antilymphangiogenic effect. Immunostaining and flow cytometry data revealed that LNs of athymic mice have higher percentages of CD11b$^+$ macrophages and CD11c$^+$ DCs compared to those of normal mice in steady state, suggesting that the T cell-deficient condition may influence other immune cell populations (Figure 3G). We interpreted this as the state of increased LNLVs in athymic mice possibly harboring more sinus-lining macrophages and DCs (Ohtani and Ohtani, 2008), which in turn would secrete more VEGFs (Kataru et al., 2009; Maruyama et al., 2005; Webster et al., 2006). Indeed, higher regional concentrations of VEGFs were observed in the LNs (Figure 3F), although their source remains to be identified.

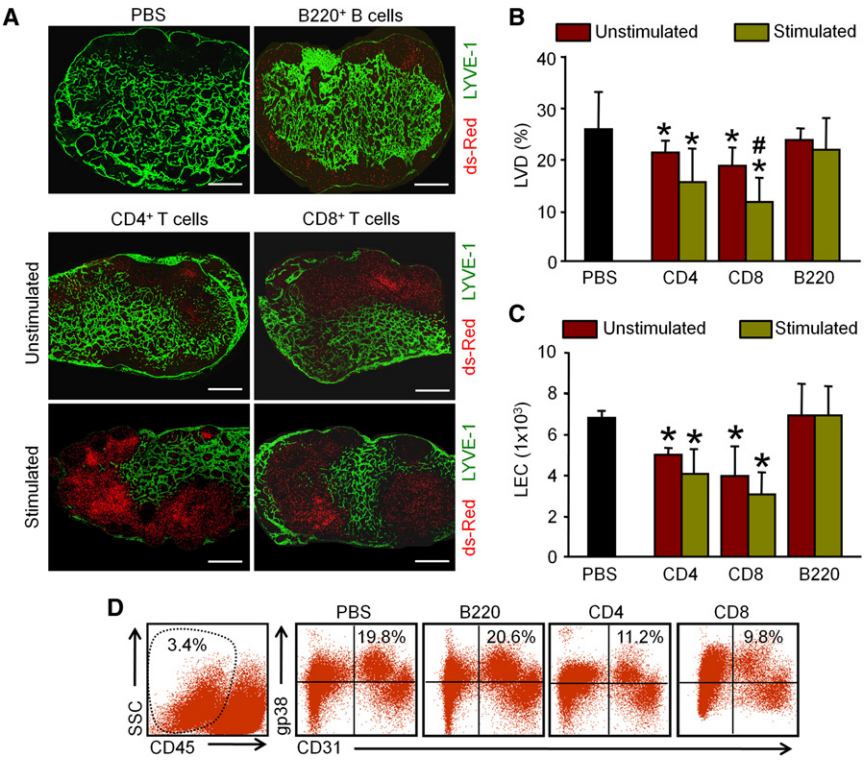

Figure 2. Suppression of LNLVs Occurs by Adoptive Transfer of CD4$^+$ and CD8$^+$ T Cells but Not of B220$^+$ B Cells

5×10^7 cells of (unstimulated or stimulated with PMA and ionomycin) CD4$^+$ T cells (CD4), CD8$^+$ T cells (CD8), or B220$^+$ B cells (B220) from ds-Red mice were adoptively transferred into athymic nude mice. PBS was injected into control mice. mLNs were sampled 2 days after transfer.

(A) Representative images showing the distribution of adoptively transferred cells (red) and LYVE-1$^+$ LVs in the midsections of mLNs from n = 4 per group in two independent experiments. Scale bars represent 500 μm.

(B) Comparison of LV density (LVD). Graph shows mean ± SD (n = 4 per group in two independent experiments). *p < 0.05 versus PBS; #p < 0.05 versus unstimulated.

(C) Comparison of LEC count by flow cytometry analysis per 1×10^6 LN cells. Graph shows mean ± SD (n = 3 per group in two independent experiments). *p < 0.05 versus PBS.

(D) Representative flow cytometry analysis of the percentage of CD31$^+$/gp38$^+$ LECs after adoptive transfer of the stimulated cells (n = 3 per group in two independent experiments).

Changes in LNLV Density in Inflammatory Conditions and Tumor

We also modulated the number and ratio of T and B cells by treatment with two inflammatory agents, LPS and Concanavalin-A (Con-A). LPS (15 μg per treatment) or Con-A (15 μg per treatment) was injected into the dorsal side of the ear skin and changes of LNLVs were examined in the draining cLN. At the peak of inflammation (3 days after injection), LPS robustly increased LNLVs (~3.1-fold), LEC percentage, and upregulated VEGFs mRNA (~2-, 1.7-, 2.4-fold increase of VEGF-A, -C, and -D, respectively, compared to PBS control), but Con A failed to increase the LNLV density and LEC percentage in cLN despite its successful induction of strong peripheral inflammation and upregulation of VEGFs (~2.7-, 1.2-, 3-fold increase of VEGF-A, -C, and -D, respectively, compared to PBS control) (Figures 4A–4C; Figure S2A). In fact, the total number of lymphocytes increased to a comparable degree between LPS and Con-A treatments, but the T cell/B cell ratio was higher in the Con-A-treated group compared with the LPS-treated group (1.57 versus 0.39) (Figure 4D). Intriguingly, Con-A, but not LPS, profoundly upregulated IFN-γ mRNA expression (Figure 4C). Moreover, IFN-γ concentration in the cell supernatant of LN tissue obtained from mice treated with Con-A were highly elevated, but not with PBS or LPS (Figure S2B).

Similar to inflammation, primary tumor is known to cause increased LNLVs in the regional LNs (Hirakawa et al., 2007; Tobler and Detmar, 2006). Therefore, we examined LNLV density in the Lewis lung carcinoma (LLC) implantation model. As expected, the ipsilateral regional iLN displayed markedly increased LYVE-1$^+$ LVs, which occupied the entire T cell zones (Figure 4E). Simultaneously, a significant reduction in the total number of LN T cells was also noticed (~62.5% reduction compared to normal LNs) (Figures 4F and 4G), reflecting an inverse relationship between LNLV density and the number of T cells.

LNLV Regression Is Attenuated by Adoptive Transfer of T Cells from IFN-γ-Deficient Mice

To determine the effect of IFN-γ on LNLVs in vivo, mice were intradermally treated with 3 μg of IFN-γ twice a day for 4 days into the ear skin. After treatment, the draining LNs were examined to measure LNLV density. IFN-γ treatment slightly but significantly reduced the LNLV density compared with PBS treatment (~30% reduction) (Figures S3A and S3C). The number of Prox-1$^+$ LECs per LV was significantly reduced upon IFN-γ treatment (~50%) (Figures S3B and S3D). Notably, Prox-1 expression was downregulated in a considerable portion of the observed LECs in the LNs treated with IFN-γ (Figure S3B).

Because we recognized IFN-γ as a candidate molecule responsible for LNLV suppression, we next performed adoptive transfer with either unstimulated or stimulated T cell subsets labeled with CFDA-SE green fluorescent that was derived from IFN-γ-deficient (*Ifng*$^{-/-}$) mice into athymic mice. Green fluorescence was detected in the LNs, indicating that successful homing of T cells had occurred. Unlike the potent LV suppression observed by the adoptive transfer of normal T cells (Figures 2A and 2B), *Ifng*$^{-/-}$ T cells failed to completely inhibit the LNLVs and remaining LVs were observed at modest frequency (Figure 5A). The overall LNLV density failed to achieve statistically significant difference when compared with PBS-treated control (Figure 5B). However, LNLV suppression still occurred in areas where *Ifng*$^{-/-}$ T cells were heavily populated. These results indicate that IFN-γ critically participates in the process of T cell-mediated LNLV suppression but also implies that

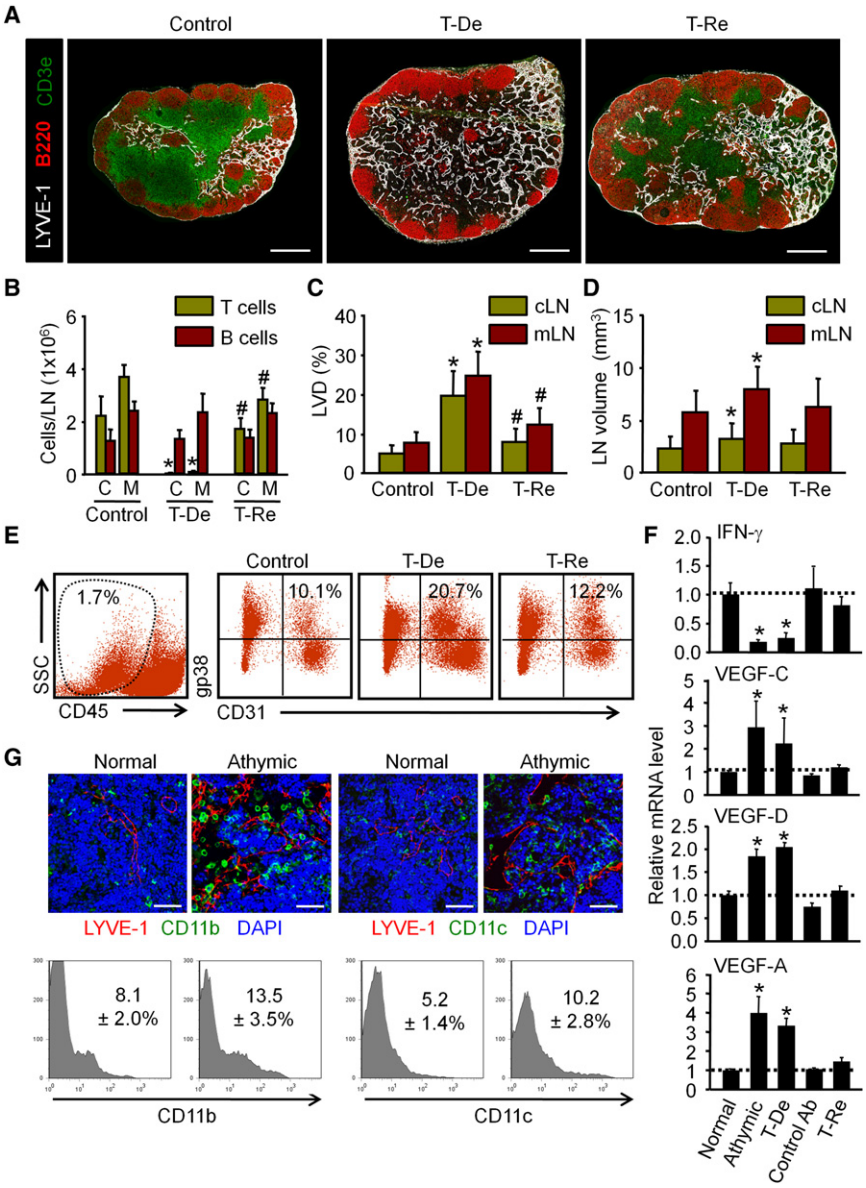

Figure 3. Reversible Changes of LNLVs with Depletion and Restoration of T Cells

BALB/c mice were intravenously injected with anti-CD3ε (1 mg/kg/day) or hamster anti-mouse IgG isotype Ab (Control) for 5 days to induce T cell depletion (T-De) and then were left untreated for 10 days to allow T cell restoration (T-Re). Cervical LN (cLN, C) and mesenteric LN (mLN, M) were sampled at day 5 (Control and T-De) and 15 (T-Re) after antibody injection.

(A) Representative images showing the distribution of $CD3\varepsilon^+$ T cells, $B220^+$ B cells, and $LYVE\text{-}1^+$ LV in the midsections of mLN from n = 5 in two independent experiments. Scale bars represent 500 μm.

(B) Comparison of numbers of T and B cells (n = 5 per group in two independent experiments). $^*p < 0.05$ versus control; $^\#p < 0.05$ versus T-De.

(C) Comparison of LV density (LVD) (n = 5 per group in two independent experiments). $^*p < 0.05$ versus control; $^\#p < 0.05$ versus T-De.

(D) Comparison of LN volume (n = 5 per group in two independent experiments). $^*p < 0.05$ versus control.

(E) Representative flow cytometry analysis of the percentage of $CD31^+/gp38^+$ LECs in the cLN (n = 4 per group in two independent experiments).

(F) Comparison of mRNA expressions of IFN-γ, VEGF-A, -C, and -D in the cLNs. Data are presented as relative fold to control after standardization with GAPDH (n = 4 per group in two independent experiments). $^*p < 0.05$ versus normal.

(G) Representative images showing the distribution of $LYVE\text{-}1^+$ LVs, $CD11b^+$ macrophages, and $CD11c^+$ DCs in the midsections of cLNs in untreated normal and athymic mice from three independent experiments. Scale bars represent 50 μm. Histograms showing populations of $CD11b^+$ macrophages and $CD11c^+$ DCs in the cLNs of untreated normal and athymic mice (n = 4 per group in two independent experiments). The graphs show mean ± SD.

IFN-γ probably is not the only molecule that is involved in this process.

Postinflammatory LNLV Regression Is Attenuated in IFN-γ-Deficient Mice

We next explored the status of LNLVs in *Ifng*$^{-/-}$ mice. Four major LNs of *Ifng*$^{-/-}$ mice were coimmunostained for LYVE-1 and PECAM-1. Compared with wild-type, all LNs from *Ifng*$^{-/-}$ mice displayed an increase in LNLV density (~1.7-fold), but no differences were observed in blood vessel density (Figure 5C and data not shown). The profiles of T and B cell populations of *Ifng*$^{-/-}$ mice were similar to those of wild-type mice in normal condition. To examine the effect of inflammation on LNLVs upon IFN-γ deficiency, *Ifng*$^{-/-}$ mice were intradermally injected with LPS into the peripheral ear skin. Three days after LPS treatment (during the peak of inflammation), cLN from both wild-type and *Ifng*$^{-/-}$ mice displayed a similar increase in LNLV density (~3.3- and ~3.5-fold in wild-type and *Ifng*$^{-/-}$, respectively) (Figures 5C and 5D). Simultaneously, the ratio of T cells to B cells was significantly decreased in wild-type, but not in *Ifng*$^{-/-}$, mice (Figure 5E). Twelve days after LPS treatment (during the resolving stage of inflammation), the increased LNLV density observed at 3 days after LPS injection had been significantly reduced in wild-type mice, whereas those of the *Ifng*$^{-/-}$ mice remained persistently increased (Figures 5C and 5D). These data indicate that IFN-γ is an important mediator with a suppressive effect on LNLVs during the baseline state and resolving stage of inflammation.

IFN-γ-Mediated LNLV Suppression Is a Primary Event

If we assume that the T cells maintain a constitutive negative-feedback signal to the prolymphangiogenic drive known to be

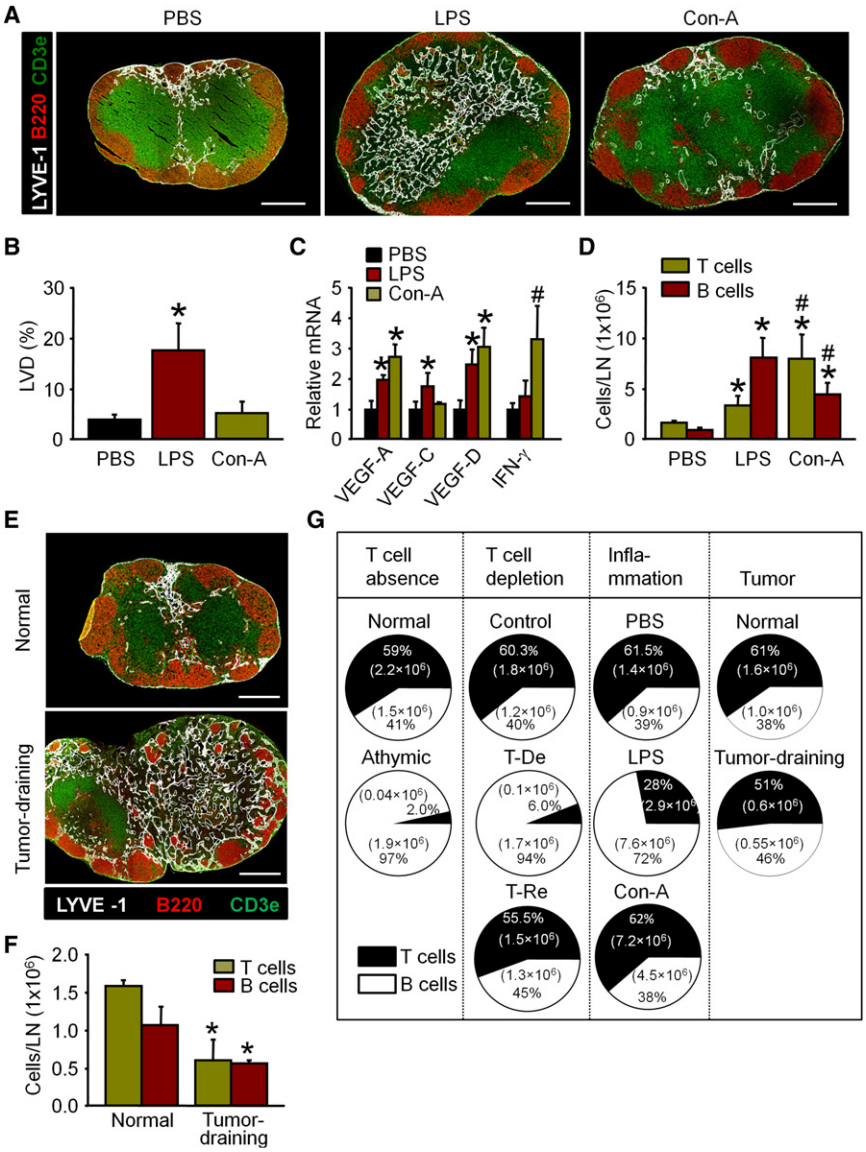

Figure 4. Alterations of LNLV Density by Modulations of T and B Cell Populations

(A–D) BALB/c mice were intradermally injected with PBS, LPS (15 μg), or Con-A (15 μg) into the dorsal side of the ear. cLNs were sampled 3 days after injection.

(A) Representative images showing distributions of CD3ε$^+$ T cells, B220$^+$ B cells, and LYVE-1$^+$ LVs in the midsections of cLNs from n = 5 in two independent experiments. Scale bars represent 500 μm.

(B) Comparison of LV density (LVD) (n = 5 per group in two independent experiments). *p < 0.05 versus PBS or Con-A.

(C) Comparison of VEGF-A, -C, -D, and IFN-γ mRNA level in cLN. Data are presented as relative fold to PBS after normalization with GAPDH (n = 4 per group in two independent experiments). *p < 0.05 versus PBS; #p < 0.05 versus LPS and PBS.

(D) Comparison of numbers of T and B cells. Each group, n = 5. *p < 0.05 versus PBS; #p < 0.05 versus LPS (n = 5 per group in two independent experiments).

(E–G) 1 × 10^6 LLC tumor cells were subcutaneously injected into the flank region of C57BL/6J mice. Tumor-draining iLNs were sampled 4 weeks after tumor implantation for immunohistochemistry and flow cytometric analysis.

(E) Representative images showing the spatial distribution of CD3ε$^+$ T cells, B220$^+$ B cells, and LYVE-1$^+$ LVs in the midsections of iLNs from n = 4 in two independent experiments. Scale bars represent 500 μm.

(F) Comparison of numbers of T and B cells (n = 4 per group in two independent experiments). *p < 0.05 versus normal.

(G) Tabular form of pie diagrams indicating the T and B cell populations in affected LNs from four different models in which the lymphocyte population is altered. Decreased T cell to B cell ratio correlates with higher LNLV density in all four models.

The graphs show mean ± SD. See also Figure S2.

produced by B cells, macrophages, and DCs, then the increased state of LNLVs we observed during various conditions of T cell depletion could simply be explained by a secondary enforcement of the prolymphangiogenic drive. Therefore it is important to identify whether the T cell-induced LNLV suppression we describe is a real primary phenomena or merely the outcome of secondary negative feedback to the prolymphangiogenic stimuli. To clarify this matter, we performed a set of bone marrow transplantions that would intercept the signal transduction of IFN-γ by selectively removing the IFN-γ receptor from either the hematopoietic cells or nonhematopoietic cells, respectively, by using IFN-γR1-deficient (*Ifngr1*$^{-/-}$) donor and wild-type (WT) recipient (*Ifngr1*$^{-/-}$:WT) or vice versa (WT:*Ifngr1*$^{-/-}$). Three days after LPS injection into the ear, marked lymphangiogenesis was observed in both types of bone marrow transplanted mice. After 12 days, however, only the *Ifngr1*$^{-/-}$:WT mice demonstrated LNLV regression similar to baseline, whereas the LNLVs of WT:*Ifngr1*$^{-/-}$ remained increased (Figures 6A and 6B). This indicates that the interference of IFN-γ signaling to prolymphangiogenic hematopoietic cells do not inhibit the ability to suppress LNLVs, but depriving the signaling to the nonhematopoietic cells (which include LECs) do. Therefore, the mechanism of IFN-γ-mediated LNLV inhibition is through direct effect that cannot be interpreted as the secondary weakening of prolymphangiogenic stimuli generated by B cells, macrophages, and DCs.

To further specify the functional independence of the effect of IFN-γ and exclude the possibility of a compensatory involvement of the prolymphangiogenic hematopoietic cells being the major mechanism of LNLV suppression, we conducted an adoptive transfer experiment in which the IFN-γ receptors only of B cells but not of T cells were selectively deleted. We performed a double adoptive transfer with T cells from dsRed mice and B cells from *Ifngr1*$^{-/-}$ mice labeled with CFDA-SE into *Rag1*$^{-/-}$ mice (which are deficient of both T and B cells). Three days after

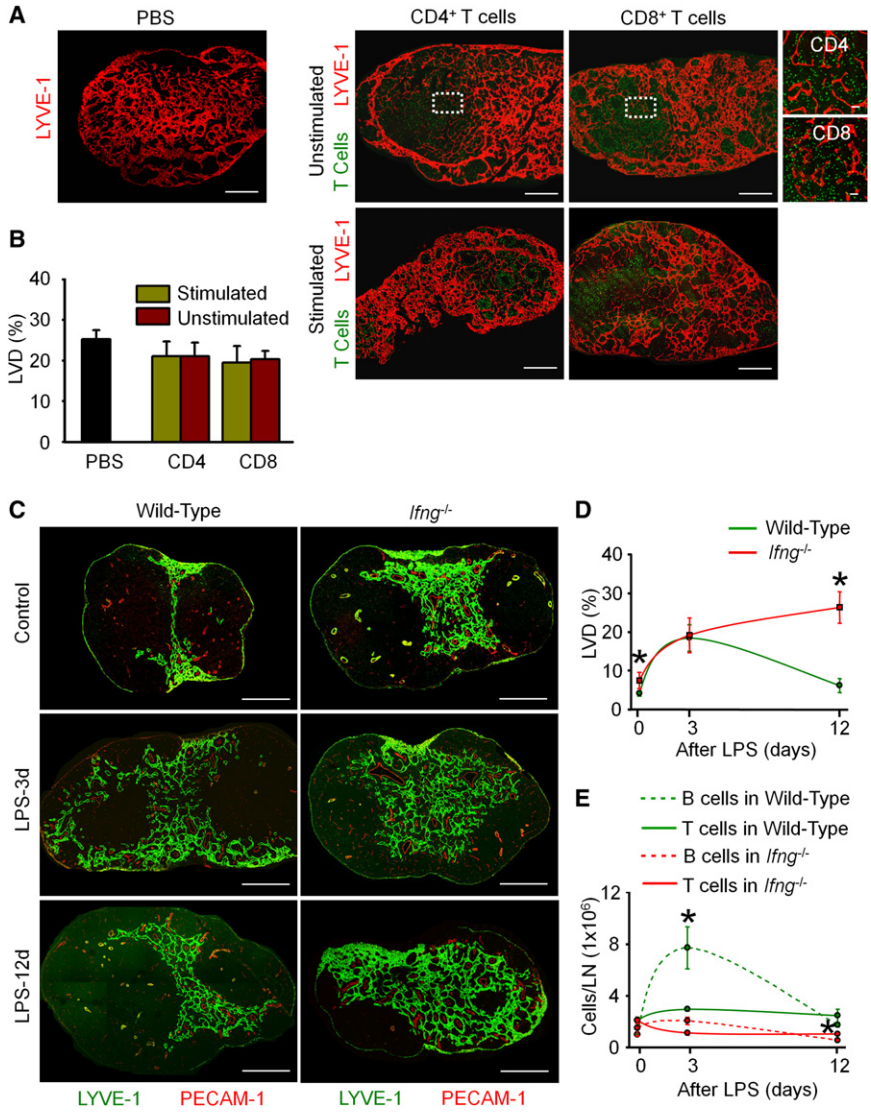

Figure 5. Adoptive Transfer of *Ifng*$^{-/-}$ T Cells Shows Incomplete LNLV Suppression, and the LNLV Regression Is Attenuated during Inflammation Resolution in the *Ifng*$^{-/-}$ Mice

(A and B) 5 × 10^7 cells of purified CD4$^+$ T cells (CD4) and CD8$^+$ T cells (CD8) either unstimulated or stimulated with PMA and ionomycin from *Ifng*$^{-/-}$ mice were labeled with CFDA-SE and adoptively transferred to athymic nude mice. PBS was injected as negative control. mLNs were sampled 2 days after transfer.

(A) Representative images showing the distribution of adoptively transferred cells (green) and LYVE-1+ LVs in the midsections of mLNs from n = 4 in two independent experiments. Scale bars represent 500 μm. Regions densely populated with T cells (indicated as white dotted line square in each inset) were viewed under high magnification.

(B) Comparison of LV density (LVD) (n = 4 per group in two independent experiments).

(C–E) Wild-type and *Ifng*$^{-/-}$ BALB/c mice were intradermally injected with LPS (15 μg) into the dorsal side of the ear. cLNs were sampled 1 day before (control) and 3 (LPS-3d) and 12 (LPS-12d) days after injection.

(C) Representative images showing the distribution of LYVE-1$^+$ LVs and PECAM-1$^+$ blood vessels in the midsections of cLNs from n = 4 in two independent experiments. Scale bars represent 500 μm.

(D) Comparison of LV density (LVD) (n = 4 per group in two independent experiments). *p < 0.05 versus wild-type.

(E) Comparison of numbers of T and B cells (n = 4 per group in two independent experiments). *p < 0.05 versus B cells in *Ifng*$^{-/-}$.

The graphs show mean ± SD. See also Figure S3.

intradermal injection of LPS into the ear, the cLNs displayed a diffused increase of LNLVs in the control (PBS only transferred) *Rag1*$^{-/-}$ mice. In contrast, strong suppression of LNLV was observed in regions where T cells reside in the double adoptive transferred *Rag1*$^{-/-}$ mice (Figures 6C and 6D), indicating that T cells can still achieve LV inhibition even under conditions in which B cells cannot be provoked by IFN-γ. Thus, the action of IFN-γ is independent of B cell activity.

IFN-γ Negatively Regulates Prox-1 Expression in LECs

Based on the inhibitory effect of T cells via IFN-γ on LNLVs observed in vivo, we expanded our investigation to the effect of T cells on primary cultured LECs in vitro. To confirm that IFN-γ mediates LV suppression, we examined LV sprouting and growth in vitro by 3-dimensional culture of LVs from mouse thoracic duct (TD) rings implanted into Matrigel (Bruyere et al., 2008). In control TD rings, sprouting tips were seen around 3 to 4 days after implantation, and robust growth of LVs from the TD ring was observed around 7–8 days. Coculturing TD rings with stimulated normal T cells resulted in very few sprouts and the majority failed to grow into vessel structures. In contrast, TDs cocultured with *Ifng*$^{-/-}$ T cells demonstrated modest sprouting and growth of LVs, but was not as robust as the negative control (Figures S4A and S4B). This indicates that the antilymphangiogenic effect of T cells occurs in an IFN-γ-dependent fashion, but also implies that pathways other than IFN-γ may be involved in this process.

We also used a cell culture insert system to coculture LECs with either CD4$^+$CD8$^+$ T cells or CD19$^+$ B cells prestimulated for IFN-γ production. After 2 days of coculture, LECs with the T cells but not B cells showed dramatically elongated cell morphology on a phase contrast microscope (Figure S4C). Interestingly, immunocytochemistry and qRT-PCR of LECs demonstrated reduced protein and mRNA expression of Prox-1 when cocultured with either CD4$^+$ or CD8$^+$ T cells but not with CD19$^+$ B cells (Figures S4C and S4D). Blocking Ab against IFN-γ partially restored LEC Prox-1 mRNA expression (Figure S4D).

To further dissect the mechanisms underlying the antilymphatic effect of IFN-γ, we treated recombinant IFN-γ to primary cultured human dermal LECs, which actively expressed both

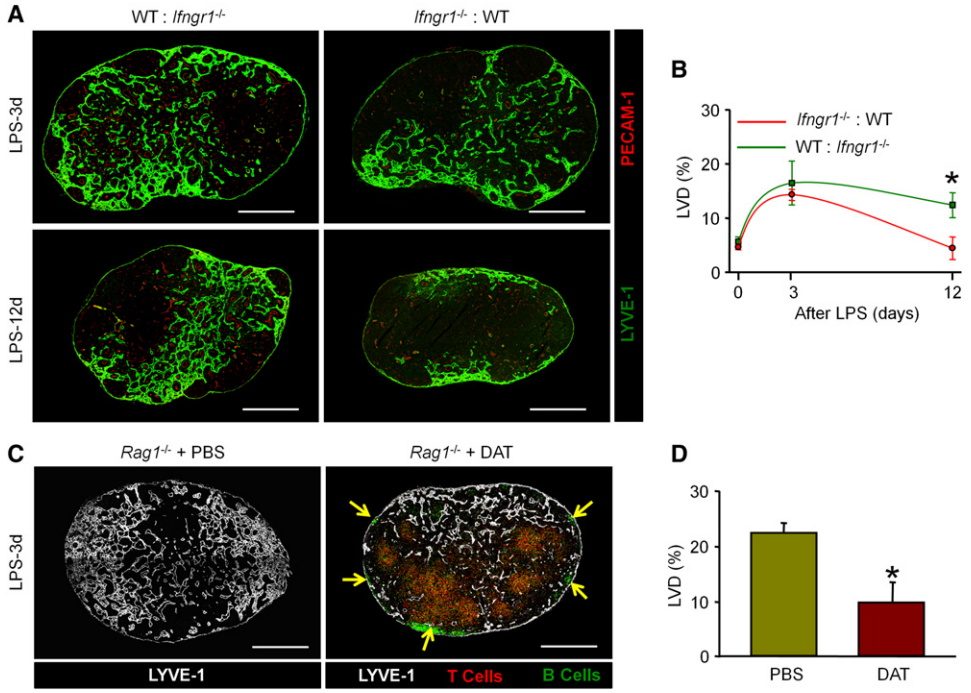

Figure 6. IFN-γ-Mediated LNLV Inhibition Is a Primary Event

(A and B) WT:*Ifngr1*$^{-/-}$ and *Ifngr1*$^{-/-}$:WT BM transplanted mice were intradermally injected with LPS (15 μg) into the dorsal side of the ear. cLNs were examined 3 (LPS-3d) and 12 (LPS-12d) days after injection.

(A) Representative images showing the distribution of LYVE-1$^+$ LVs and PECAM-1$^+$ blood vessels in the midsections of cLNs from n = 5 in two independent experiments. Scale bars represent 500 μm.

(B) Comparison of LV density (LVD) (n = 5 per group in two independent experiments). *p < 0.05 versus WT:*Ifngr1*$^{-/-}$.

(C and D) 3 × 10^7 cells of purified T cells (ds-Red) and *Ifngr1*$^{-/-}$ B cells (CFDA-SE labeled) were adoptively transferred to *Rag1*$^{-/-}$ mice (*Rag1*$^{-/-}$ +DAT; double adoptive transfer). PBS was injected as negative control (*Rag1*$^{-/-}$ +PBS). LPS (15 μg) was injected intradermally into the dorsal side of the ear to all mice. cLNs were sampled 3 days (LPS-3d) after LPS injection.

(C) Representative images showing the distribution of LYVE-1$^+$ LVs, ds-Red$^+$ T cells, and CFDA-SE-labeled B cells (yellow arrows) in the midsections of cLNs from n = 4 per group in two independent experiments. Scale bars represent 500 μm.

(D) Comparison of LV density (LVD) (n = 4 per group in two independent experiments). Each group, n = 4. *p < 0.05 versus *Rag1*$^{-/-}$ +PBS.

The graphs show mean ± SD.

IFN-γ receptor-1 (IFNGR1) and IFNGR2 (Figure S4E). The mRNA expression of IRF1, an IFN-γ-responsive transcription factor (Schroder et al., 2004), was highly upregulated (~13.2-fold) after IFN-γ treatment, reflecting the responsiveness of LECs to IFN-γ (data not shown). IFN-γ at a concentration of 1 μg/ml did not show a measureable cytotoxic effect on LECs (Figure S4F), but markedly elongated extensions of actin stress fibers were observed 24 hr after treatment (Figure 7A). Immunocytochemistry demonstrated a considerable reduction of Prox-1 signal in the IFN-γ-treated LECs (Figure 7A). Immunoblot analyses confirmed that the Prox-1 protein was reduced with IFN-γ treatment (Figure 7B). Correspondingly, the mRNA of Prox-1 was also decreased by IFN-γ treatment in a dose-dependent manner (Figure 7C), indicating that IFN-γ negatively regulates the expression of Prox-1 at the transcriptional level. In addition to Prox-1, mRNA of several LEC-specific genes, such as LYVE-1 and podoplanin, were also suppressed by IFN-γ (Figures 7D and 7E). However, downregulation of Prox-1 rapidly occurred within 2 hr after IFN-γ treatment, whereas the suppression of LYVE-1 and podoplanin was observed after 24 hr (data not shown). These results suggest that IFN-γ acts as a suppressor of lymphatic growth by downregulating the expression of LEC-specific genes.

We next investigated several potential signaling pathways that might be involved in this IFN-γ-induced downregulation of Prox-1. Previous studies have shown that various signaling pathways, including MAPK, ERK, PI3K, IKK, and JAK-STAT, can be stimulated by IFN-γ (Gough et al., 2008; Schroder et al., 2004). Therefore, we pretreated LECs with specific inhibitors that are known to block each signaling pathway and searched for any alterations in the IFN-γ-induced Prox-1 downregulation. Only piceatannol, a JAK1 inhibitor (Geahlen and McLaughlin, 1989), selectively blocked the IFN-γ-induced Prox-1 downregulation in a dose-dependent manner, whereas PI3K, MEK, or IKK inhibitors did not show significant influence over the IFN-γ-induced Prox-1 downregulation (Figures S4G and S4H). These data indicate JAK1 as a crucial participant of the signaling pathway mediating the IFN-γ-dependent Prox-1 downregulation observed in LECs. Because a major downstream effecter of JAK1 is the STAT1 transcription factor, we examined whether STAT1 is also involved in the IFN-γ-induced Prox-1 downregulation. We used (-)-epigallocatechin-3-gallate

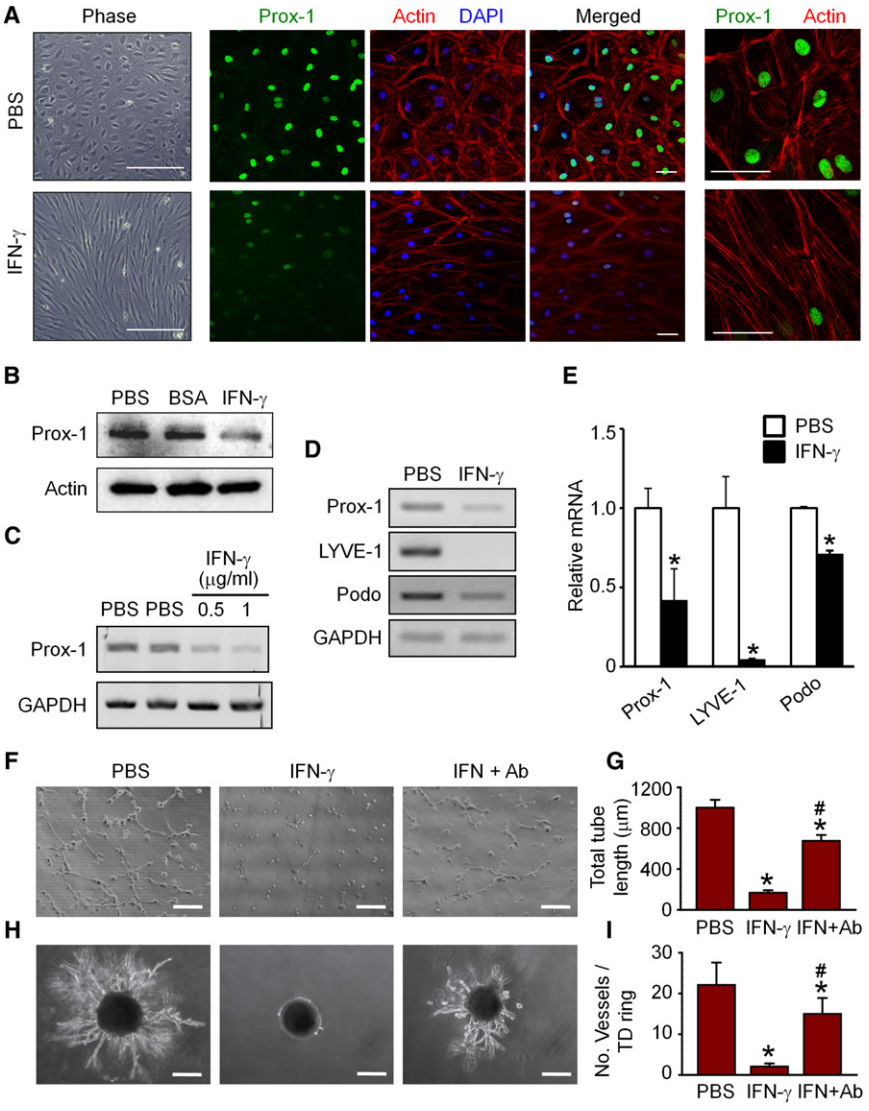

Figure 7. IFN-γ Negatively Regulates Prox-1 Expression in LECs and In Vitro Lymphangiogenesis

(A–E) Primary cultured human dermal LECs were treated with PBS, BSA (1 μg/ml/day), or IFN-γ (1 μg/ml/day) every 24 hr for 3 days and were sampled.

(A) Left: Phase contrast images showing LEC morphology from n = 3 in two independent experiments. Scale bars represent 50 μm. Middle and right: Confocal images showing Prox-1, actin, and DAPI in LECs. Scale bars represent 20 μm.

(B) Immunoblotting for Prox-1 expression in PBS-, BSA-, and IFN-γ-treated LECs from n = 3 per group in two independent experiments.

(C) Semiquantitative RT-PCR for Prox-1 mRNA after IFN-γ treatment in two concentrations (n = 3 per group in two independent experiments).

(D) Semiquantitative RT-PCR for Prox-1, LYVE-1, podoplanin (Podo), and GAPDH mRNAs (n = 3 per group in two independent experiments).

(E) Comparison of Prox-1, LYVE-1, and podoplanin mRNA levels from IFN-γ-treated LECs via quantitative RT-PCR. Data are presented as relative folds to PBS-treated control group after standardization with GAPDH (n = 4 per group in two independent experiments). *p < 0.05 versus PBS.

(F and G) About 3 × 10^4 LECs were seeded into Matrigel with or without IFN-γ (1 μg/ml) and IFN-γ blocking Ab (5 μg/ml) and were incubated for 24 hr.

(F) Representative phase contrast images of LEC tube formation assay with media each added with PBS, IFN-γ alone, or IFN-γ in combination with IFN-γ-blocking Ab from n = 4 per group in two independent experiments. Scale bars represent 50 μm.

(G) Comparison of the total length of tube formation (exceeding 20 μm in diameter), calculated from 10 random field images from each individual experiment (n = 4 per group in two independent experiments). *p < 0.05 versus PBS; #p < 0.05 versus IFN-γ.

(H and I) Excised rings of thoracic ducts (TD) were implanted into Matrigel and cultured for 2 weeks with normal condition media alone or with media plus IFN-γ (1 μg/ml), with or without IFN-γ-blocking Ab (5 μg/ml) on day 0 and day 7 and incubated for 2 weeks.

(H) Representative phase contrast images showing lymphatic sprouts from n = 4 per group in two independent experiments. Scale bars represent 50 μm.

(I) Comparison of number of lymphatic sprouts (exceeding 20 μm length) per TD (n = 4 per group in two independent experiments). *p < 0.05 versus PBS; #p < 0.05 versus IFN-γ.

The graphs show mean ± SD. See also Figures S4 and S5.

(EGCG) that is known to specifically inhibit the phosphorylation of STAT1 but not STAT3 (Tedeschi et al., 2002). Pretreatment of EGCG significantly restored the immunoreactivity and mRNA expression of Prox-1 that was suppressed by IFN-γ. In contrast, pretreatment of (-)-epigallocatechin (EGC), a structurally similar chemical to EGCG, failed to reverse the IFN-γ-induced Prox-1 downregulation (Figures S4I and S4J). Collectively, these results demonstrate that the JAK1-STAT1 pathway is critically involved in the IFN-γ-mediated Prox-1 downregulation in LECs.

IFN-γ Negatively Regulates In Vitro Lymphangiogenesis

We next examined the effect of IFN-γ on tube formation of LECs in vitro. Successful tube formation was observed as early as 6 hr after plating LECs on Matrigel-coated dishes in normal growth condition. However, adding IFN-γ (1 μg/ml) to freshly plated LECs caused a decrease in tube formation (~80% reduction compared with PBS-treated controls) for at least 24 hr (Figures 7F and 7G). Reversibly, IFN-γ-neutralizing antibody suppressed the inhibitory effect of IFN-γ on tube formation (Figures 7F and 7G). It has been previously reported that budding and sprouting of LECs require Prox-1 function (Wigle and Oliver, 1999). Therefore, to further corroborate the antilymphangiogenic effect of IFN-γ, we examined the effect of IFN-γ on LV sprouting and growth in vitro by 3-dimensional culture of LVs from mouse thoracic duct (TD) rings implanted into Matrigel (Bruyere et al., 2008). Without adding IFN-γ, sprouting tips were seen around 3 to 4 days after implantation, and robust growth of LVs from

the TD ring was observed around 7–10 days. However, providing IFN-γ at a concentration of 1 μg/ml completely inhibited the LV sprouting and growth from TD rings; this inhibitory effect was rescued by adding IFN-γ-neutralizing Ab (Figures 7H and 7I). The IFN-γ-treated TD rings started to sprout and grow normally into vessel structures after replacing the media without IFN-γ (data not shown), indicating that IFN-γ-dependent inhibition of LV sprouting and growth is a reversible process.

Increased LNLV Density Promotes the Recruitment of Antigen-Carrying DCs

Because the increase of LNLVs was reported to stimulate DC recruitment into LNs (Angeli et al., 2006), we wondered whether the state of highly dense LNLVs induced by T cell deficiency could promote the recruitment of antigen-carrying DCs. Ear drainage to the cLNs of athymic and normal control mice was examined 2 days after 1 μm fluorescent microspheres were intradermally injected into the ear. In the control cLNs, the microspheres were densely distributed mostly along the LYVE-1$^+$ LVs of the subcapsular area but were only scarcely found in the cortical regions (Figure S5A). In contrast, cLNs in athymic mice showed abundant microspheres both in the cortical regions and along the LYVE-1$^+$ LVs of the subcapsular area, suggesting that the microspheres in the LNs of athymic mice migrated relatively deeper into the paracortex and cortex compared with those in control mice (Figure S5A). In the cortical regions of cLNs in athymic mice, a fair amount of the microspheres were colocalized with CD11c$^+$ DCs, indicating the presence of microsphere-carrying DCs in these regions (Figure S5A). Most of these microsphere-carrying DCs were in close contact with the dense LYVE1$^+$ LNLVs, suggesting that LNLVs are major conduits for these antigen-carrying DCs. These data suggest a scenario where the absence of T cells leads to an increase in LNLV density, which thereby facilitates the physical interaction between antigen-carrying DCs and less populated T cells (Figure S5B).

DISCUSSION

Here we provide evidence that the T cells negatively regulate LNLVs mainly through IFN-γ. We also suggest a scenario where the antilymphatic T cells maintain a homeostatic balance against their counterpart prolymphatic B cells, and that the T/B cell ratio is a key modulating factor that determines the LNLV density. If the T cell-dependent antilymphatic drive is weakened because of a decline of intranodal T cell count as shown in our study, a relative augmentation of prolymphatic components would occur even without necessarily increasing their quantities. Consequently, the homeostatic balance would be shifted toward a state of excessive secretion of B cell-derived VEGFs that is unopposed, tilting the balance toward the direction of overall promotion of LNLV growth. However, T cell-mediated LNLV suppression is the primary event instead of a mere endpoint of compensation, as shown by the fact that T cells still accomplish LNLV inhibition when B cells were unresponsive to IFN-γ.

An example of our hypothesis is the change in LNLVs observed in inflammatory models. Our results demonstrated that LPS-mediated acute inflammation induced an increase in the B cells/T cells ratio that was accompanied by LNLV growth and penetration into T cell zones. In contrast, Con-A (T cell mitogen)-mediated acute inflammation failed to promote the growth of LNLVs, despite strong inflammatory reactions at the ear skin and increased B cell number and VEGFs in LNs. However, Con-A induced a robust proliferation of both T cells and B cells in a parallel manner, and thus the T/B cell ratio was maintained relatively constant to the basal level with a concurrent and balanced increase of pro- and antilymphangiogenic factors. These results strengthen our proposed concept that the negative regulation by T cells is deeply involved in the mechanism causing an increase of LNLVs during inflammation. We then questioned whether the LPS-induced increase of LNLVs would regress back to the basal state as inflammation subsides and, if so, whether the altered T cell/B cell ratio could serve as a direct cause for such an effect. Given that the T cell/B cell ratio is minimal whereas LNLV density is maximal at the peak of inflammation, and vice versa for both preinduction and postresolution of inflammation, we deduce the T cells are involved in not only the growth but also the regression of LNLVs during the evolution of inflammation. Similar observations in the draining LNs of arthritic joints displaying decreased T cells (Rodriguez-Palmero et al., 1999) and increased LNLVs (Guo et al., 2009) were reported during the latent period of arthritis in different rodent models. Collectively, we consider the entire process as a balance between prolymphatic and antilymphatic components that is roughly represented by the T cell/B cell ratio; this hypothesis is supported by our observations in athymic mice, pharmacologically T-De and T-Re mice, LPS- or Con-A-induced inflammation models, and experimental tumor-implanted mice.

In our study, we tried to dissect the molecule(s) and signaling pathway(s) the T cells adopt to regulate LNLVs. We consider IFN-γ as our most important candidate, because *Ifng*$^{-/-}$ mice showed an increased baseline amount of LNLVs, and the further enhanced growth of LNLVs induced by acute inflammation failed to subside during the resolving stage of inflammation. However, as we have demonstrated by the adoptive transfer and TD ring coculture with T cells derived from *Ifng*$^{-/-}$ mice, the inactivation of IFN-γ alone cannot completely neutralize the T cell-mediated antilymphatic effect. This suggests that other yet unknown T cell-originating factors probably also participate in LNLV suppression and may compensate for the absence of IFN-γ. We hope that subsequent studies will further elucidate other involved signaling pathways.

We also showed that IFN-γ treatment causes the downregulation of Prox-1, LYVE-1, and podoplanin in LECs and strongly repress lymphatic sprouting and growth in vitro. Prox-1, a major LEC-specific transcription factor, plays an important role in the survival, maintenance, and proliferation of LECs (Johnson et al., 2008; Petrova et al., 2002; Tammela and Alitalo, 2010; Wigle and Oliver, 1999). Multiple effects of IFN-γ in regulating the process of immunity are known to be modulated through the JAK-STAT pathway (Hu and Ivashkiv, 2009). Consistently, our results show that the effects of IFN-γ on LECs are mediated through serial events of signaling by IFN-γ via IFNGR1 and/or IFNGR2, JAK, and STAT1 phosphorylation, suggesting that JAK1-STAT1 signaling is a pivotal pathway involved in the IFN-γ-mediated Prox-1 downregulation.

Another important finding of this study is that the elevated LV density in T cell-deficient LNs promoted the recruitment of

antigen-carrying DCs into the LNs. LNLVs are used as conduits to facilitate the physical interaction between antigen-carrying DCs and their corresponding T cells (Catron et al., 2004; Itano and Jenkins, 2003; von Andrian and Mempel, 2003). Unlike in normal mice, in the athymic mice we observed both the antigen and antigen-carrying DCs being abundantly distributed throughout the entire LNLV, including those situated in the deep cortex. This indicates that enhanced LNLVs subjected to the environment of T cell insufficiency promote the recruitment of antigen and antigen-carrying DCs. Similar to the aforementioned B cell-dependent growth of LNLVs and subsequent recruitment of DCs, these serial events can be interpreted as a dynamic feedback circuit designed to offer more opportunities to the DCs to meet the less populated T cells. Furthermore, it has been recently reported that LECs have a function of presenting endogenous antigen and are involved in the modulation of peripheral immune tolerance (Cohen et al., 2010). This implies that the T cells may serve as one of the biological moderators to orchestrate the entire immune system by regulating LNLVs.

In conclusion, our findings shed light on the previously unknown role of T cells being a major regulator of LNLVs. Both the T cells and B cells modulate the LNLV density but in opposing directions. In the steady state of the LN microenvironment, B cells and APCs enhance LNLV growth through soluble factors such as VEGFs, whereas T cells suppress LNLV growth via soluble factors like IFN-γ to maintain the balance at homeostasis. However, a condition causing a decline in the T cell/B cell ratio, such as in acute inflammation, upsets the balance between the two opposite forces and promotes LNLV growth. This event would promote the subsequent recruitment of antigen-carrying DCs, allowing more efficient interaction with the less populated T cells. We also identified IFN-γ secreted by T cells as an antilymphatic growth cytokine, which downregulates lymphangiogenic molecules, such as Prox-1, in LECs. Considering the importance of LNLVs in many aspects of immunity, our findings of LNLVs being regulated by T cells may be applied to develop more efficient vaccines or widen our knowledge in fields of immune-compromised pathologies and autoimmune disorders.

EXPERIMENTAL PROCEDURES

Mice and Treatments

Specific-pathogen-free C57BL/6J, BALB/c, athymic nude mice (BALB/c, CbyJ.Cg-*Foxn1*^{nu}/J), ds-Red fluorescent mice (C57BL/6J), *Ifng*$^{-/-}$ mice (C57BL/6J and BALB/c), *Ifngr1*$^{-/-}$ mice (C57BL/6J), and *Rag1*$^{-/-}$ mice (C57BL/6J) were purchased from Jackson Laboratory and bred in our pathogen-free animal facility. All animals were fed with a standard normal diet (PMI Lab Diet) ad libitum with free access to water. Seven- to eight-week-old male mice were used for this study unless otherwise specifically indicated. Animal care and experimental procedures were performed with the approval of the Animal Care Committee of KAIST.

Flow Cytometric Analysis and Histological and Morphologic Analyses

Flow cytometric analysis of LNs, fluorescent immunohistochemistry of LN tissue sections, and immunocytochemistry of cultured LECs were performed with specific primary and secondary antibodies as described in detail in Supplemental Experimental Procedures.

Purification of Lymphocytes for Adoptive Transfer

Spleens from ds-Red or *Ifng*$^{-/-}$ or *Ifngr1*$^{-/-}$ mice were excised and single-cell suspensions were prepared by pulverizing the spleens against a 40 μm nylon cell strainer into FACS buffer. RBCs were lysed with RBC lysis buffer (Sigma-Aldrich). Cells were washed with MACS buffer and counted with a hemocytometer, and equal numbers of cells were incubated with biotin-conjugated anti-mouse CD4, CD8, CD3ε, and B220 antibodies (BD Biosciences) for 30 min on ice. Cells were washed two to three times and incubated with magnetic-conjugated biotin Ab (Miltenyi Biotec) for 20 min on ice. CD4$^+$, CD8$^+$, CD3ε$^+$, or B220$^+$ cell populations were enriched with a magnetic cell sorter (MACS) (Miltenyi Biotec) according to the manufacturer's instructions. The purities of the cells were more than 93% according to flow cytometric analysis. Then the cells were stimulated with PMA (10 ng/ml) (Sigma-Aldrich) and ionomycin (200 ng/ml) (Sigma-Aldrich) for 2 hr in a 5% CO_2 incubator for IFN-γ production (whenever necessary). 5 × 10^7 cells of the stimulated or unstimulated CD4$^+$, CD8$^+$, CD3ε$^+$, or B220$^+$ cells were adoptively transferred intravenously into athymic nude or *Rag1*$^{-/-}$ mice via the tail vein. Two days after transfer, all major LNs were isolated for subsequent analyses.

Reagent Treatments

Systemic depletion of T cells (T-De) was performed by intravenous administration of anti-mouse CD3ε monoclonal Ab (1 mg/kg/day for 5 days; Clone 145-2C11; ATCC). As a control, the same amount of hamster anti-mouse IgG isotype Ab (R&D Systems) was administered in the same manner. After Ab treatment, the mice were left without any further treatment for 10 days to allow T cell restoration (T-Re). For generation of acute inflammation in the ear skin, a single injection of LPS (15 μg in 10 μl PBS) (from *Escherichia coli* 0111:B4, Sigma-Aldrich) or Con-A (15 μg in 10 μl PBS; Sigma-Aldrich) was intradermally administered with a 31-gauge syringe (BD ultra-fine II, Becton, Dickinson and Company) into the dorsal side of the ear. Ear-draining cLNs were collected at the indicated day. To examine the effect of IFN-γ in vivo, 3 μg of recombinant mouse IFN-γ (R&D Systems) was intradermally administered twice a day for 4 days into the dorsal side of the ear.

Cell Culture, Reagent Treatment, and Visualizing Antigen Mobility in LNs

These procedures were performed as described in detail in Supplemental Experimental Procedures.

Statistics

Values are presented as mean ± standard deviation (SD). Significant differences between means were determined by an analysis of variance followed by the Student-Newman-Keuls test. Statistical significance was set at $p < 0.05$.

SUPPLEMENTAL INFORMATION

Supplemental Information includes Supplemental Experimental Procedures and five figures and can be found with this article online at doi:10.1016/j.immuni.2010.12.016.

ACKNOWLEDGMENTS

We thank J.S. Hong and E.S. Lee for their technical assistance. This work was supported by the grant (R2009-0079390, G.Y.K.) of Korea Science and Engineering Foundation (KOSEF) and the WCU grant (R31-2009-000-10071-0) funded by the MEST, Korea. R.P.K., H.K., C.J., D.K.C., B.I.K, Y.-K.K., S.-H.L., and G.Y.K. designed, organized, and performed the experiments, analyzed the data, generated the figures, and wrote the manuscript. M.K. and S.G. performed flow cytometry and MACS sorting.

Received: May 18, 2010
Revised: October 5, 2010
Accepted: December 20, 2010
Published online: January 20, 2011

REFERENCES

Alvarez, D., Vollmann, E.H., and von Andrian, U.H. (2008). Mechanisms and consequences of dendritic cell migration. Immunity *29*, 325–342.

Angeli, V., Ginhoux, F., Llodra, J., Quemeneur, L., Frenette, P.S., Skobe, M., Jessberger, R., Merad, M., and Randolph, G.J. (2006). B cell-driven lymphangiogenesis in inflamed lymph nodes enhances dendritic cell mobilization. Immunity *24*, 203–215.

Bruyere, F., Melen-Lamalle, L., Blacher, S., Roland, G., Thiry, M., Moons, L., Frankenne, F., Carmeliet, P., Alitalo, K., Libert, C., et al. (2008). Modeling lymphangiogenesis in a three-dimensional culture system. Nat. Methods *5*, 431–437.

Catron, D.M., Itano, A.A., Pape, K.A., Mueller, D.L., and Jenkins, M.K. (2004). Visualizing the first 50 hr of the primary immune response to a soluble antigen. Immunity *21*, 341–347.

Chyou, S., Ekland, E.H., Carpenter, A.C., Tzeng, T.C., Tian, S., Michaud, M., Madri, J.A., and Lu, T.T. (2008). Fibroblast-type reticular stromal cells regulate the lymph node vasculature. J. Immunol. *181*, 3887–3896.

Cohen, J.N., Guidi, C.J., Tewalt, E.F., Qiao, H., Rouhani, S.J., Ruddell, A., Farr, A.G., Tung, K.S., and Engelhard, V.H. (2010). Lymph node-resident lymphatic endothelial cells mediate peripheral tolerance via Aire-independent direct antigen presentation. J. Exp. Med. *207*, 681–688.

Dalton, D.K., Pitts-Meek, S., Keshav, S., Figari, I.S., Bradley, A., and Stewart, T.A. (1993). Multiple defects of immune cell function in mice with disrupted interferon-gamma genes. Science *259*, 1739–1742.

Drayton, D.L., Liao, S., Mounzer, R.H., and Ruddle, N.H. (2006). Lymphoid organ development: From ontogeny to neogenesis. Nat. Immunol. *7*, 344–353.

Fathallah-Shaykh, H.M., Zhao, L.J., Kafrouni, A.I., Smith, G.M., and Forman, J. (2000). Gene transfer of IFN-gamma into established brain tumors represses growth by antiangiogenesis. J. Immunol. *164*, 217–222.

Gately, M.K., Warrier, R.R., Honasoge, S., Carvajal, D.M., Faherty, D.A., Connaughton, S.E., Anderson, T.D., Sarmiento, U., Hubbard, B.R., and Murphy, M. (1994). Administration of recombinant IL-12 to normal mice enhances cytolytic lymphocyte activity and induces production of IFN-gamma in vivo. Int. Immunol. *6*, 157–167.

Geahlen, R.L., and McLaughlin, J.L. (1989). Piceatannol (3,4,3′,5′-tetrahydroxy-trans-stilbene) is a naturally occurring protein-tyrosine kinase inhibitor. Biochem. Biophys. Res. Commun. *165*, 241–245.

Gough, D.J., Levy, D.E., Johnstone, R.W., and Clarke, C.J. (2008). IFNgamma signaling—Does it mean JAK-STAT? Cytokine Growth Factor Rev. *19*, 383–394.

Gretz, J.E., Anderson, A.O., and Shaw, S. (1997). Cords, channels, corridors and conduits: Critical architectural elements facilitating cell interactions in the lymph node cortex. Immunol. Rev. *156*, 11–24.

Guo, R., Zhou, Q., Proulx, S.T., Wood, R., Ji, R.C., Ritchlin, C.T., Pytowski, B., Zhu, Z., Wang, Y.J., Schwarz, E.M., et al. (2009). Inhibition of lymphangiogenesis and lymphatic drainage via vascular endothelial growth factor receptor 3 blockade increases the severity of inflammation in a mouse model of chronic inflammatory arthritis. Arthritis Rheum. *60*, 2666–2676.

Halin, C., Tobler, N.E., Vigl, B., Brown, L.F., and Detmar, M. (2007). VEGF-A produced by chronically inflamed tissue induces lymphangiogenesis in draining lymph nodes. Blood *110*, 3158–3167.

Hirakawa, S., Brown, L.F., Kodama, S., Paavonen, K., Alitalo, K., and Detmar, M. (2007). VEGF-C-induced lymphangiogenesis in sentinel lymph nodes promotes tumor metastasis to distant sites. Blood *109*, 1010–1017.

Hu, X., and Ivashkiv, L.B. (2009). Cross-regulation of signaling pathways by interferon-gamma: Implications for immune responses and autoimmune diseases. Immunity *31*, 539–550.

Ibe, S., Qin, Z., Schuler, T., Preiss, S., and Blankenstein, T. (2001). Tumor rejection by disturbing tumor stroma cell interactions. J. Exp. Med. *194*, 1549–1559.

Itano, A.A., and Jenkins, M.K. (2003). Antigen presentation to naive CD4 T cells in the lymph node. Nat. Immunol. *4*, 733–739.

Johnson, N.C., Dillard, M.E., Baluk, P., McDonald, D.M., Harvey, N.L., Frase, S.L., and Oliver, G. (2008). Lymphatic endothelial cell identity is reversible and its maintenance requires Prox1 activity. Genes Dev. *22*, 3282–3291.

Junt, T., Scandella, E., and Ludewig, B. (2008). Form follows function: Lymphoid tissue microarchitecture in antimicrobial immune defence. Nat. Rev. Immunol. *8*, 764–775.

Kataru, R.P., Jung, K., Jang, C., Yang, H., Schwendener, R.A., Baik, J.E., Han, S.H., Alitalo, K., and Koh, G.Y. (2009). Critical role of CD11b+ macrophages and VEGF in inflammatory lymphangiogenesis, antigen clearance, and inflammation resolution. Blood *113*, 5650–5659.

Kim, K.E., Koh, Y.J., Jeon, B.H., Jang, C., Han, J., Kataru, R.P., Schwendener, R.A., Kim, J.M., and Koh, G.Y. (2009). Role of CD11b+ macrophages in intraperitoneal lipopolysaccharide-induced aberrant lymphangiogenesis and lymphatic function in the diaphragm. Am. J. Pathol. *175*, 1733–1745.

Liao, S., and Ruddle, N.H. (2006). Synchrony of high endothelial venules and lymphatic vessels revealed by immunization. J. Immunol. *177*, 3369–3379.

Maruyama, K., Ii, M., Cursiefen, C., Jackson, D.G., Keino, H., Tomita, M., Van Rooijen, N., Takenaka, H., D'Amore, P.A., Stein-Streilein, J., et al. (2005). Inflammation-induced lymphangiogenesis in the cornea arises from CD11b-positive macrophages. J. Clin. Invest. *115*, 2363–2372.

Mueller, S.N., and Germain, R.N. (2009). Stromal cell contributions to the homeostasis and functionality of the immune system. Nat. Rev. Immunol. *9*, 618–629.

Ohtani, O., and Ohtani, Y. (2008). Structure and function of rat lymph nodes. Arch. Histol. Cytol. *71*, 69–76.

Petrova, T.V., Makinen, T., Makela, T.P., Saarela, J., Virtanen, I., Ferrell, R.E., Finegold, D.N., Kerjaschki, D., Yla-Herttuala, S., and Alitalo, K. (2002). Lymphatic endothelial reprogramming of vascular endothelial cells by the Prox-1 homeobox transcription factor. EMBO J. *21*, 4593–4599.

Randolph, G.J., Angeli, V., and Swartz, M.A. (2005). Dendritic-cell trafficking to lymph nodes through lymphatic vessels. Nat. Rev. Immunol. *5*, 617–628.

Rodriguez-Palmero, M., Pelegri, C., Ferri, M.J., Castell, M., Franch, A., and Castellote, C. (1999). Alterations of lymphocyte populations in lymph nodes but not in spleen during the latency period of adjuvant arthritis. Inflammation *23*, 153–165.

Ruegg, C., Yilmaz, A., Bieler, G., Bamat, J., Chaubert, P., and Lejeune, F.J. (1998). Evidence for the involvement of endothelial cell integrin alphaVbeta3 in the disruption of the tumor vasculature induced by TNF and IFN-gamma. Nat. Med. *4*, 408–414.

Schroder, K., Hertzog, P.J., Ravasi, T., and Hume, D.A. (2004). Interferon-gamma: An overview of signals, mechanisms and functions. J. Leukoc. Biol. *75*, 163–189.

Shao, X., and Liu, C. (2006). Influence of IFN-alpha and IFN-gamma on lymphangiogenesis. J. Interferon Cytokine Res. *26*, 568–574.

Tammela, T., and Alitalo, K. (2010). Lymphangiogenesis: Molecular mechanisms and future promise. Cell *140*, 460–476.

Tedeschi, E., Suzuki, H., and Menegazzi, M. (2002). Antiinflammatory action of EGCG, the main component of green tea, through STAT-1 inhibition. Ann. N Y Acad. Sci. *973*, 435–437.

Tewari, K., Nakayama, Y., and Suresh, M. (2007). Role of direct effects of IFN-gamma on T cells in the regulation of CD8 T cell homeostasis. J. Immunol. *179*, 2115–2125.

Tobler, N.E., and Detmar, M. (2006). Tumor and lymph node lymphangiogenesis—Impact on cancer metastasis. J. Leukoc. Biol. *80*, 691–696.

von Andrian, U.H., and Mempel, T.R. (2003). Homing and cellular traffic in lymph nodes. Nat. Rev. Immunol. *3*, 867–878.

Webster, B., Ekland, E.H., Agle, L.M., Chyou, S., Ruggieri, R., and Lu, T.T. (2006). Regulation of lymph node vascular growth by dendritic cells. J. Exp. Med. *203*, 1903–1913.

Whitmire, J.K., Tan, J.T., and Whitton, J.L. (2005). Interferon-gamma acts directly on CD8+ T cells to increase their abundance during virus infection. J. Exp. Med. *201*, 1053–1059.

Wigle, J.T., and Oliver, G. (1999). Prox1 function is required for the development of the murine lymphatic system. Cell *98*, 769–778.